Front. Earth Sci. 2025, 19(2): 304–321
https://doi.org/10.1007/s11707-025-1151-4

RESEARCH ARTICLE

Improved annual forest cover maps in Oklahoma from analyses of PALSAR-2, Landsat, and LiDAR data sets during 2015–2021

Yuan YAO[1], Xiangming XIAO (✉)[1], Yuanwei QIN[2,1], Jie WANG[3], Chenchen ZHANG[1], Gregory S. NEWMAN[1], Li PAN[1], Cheng MENG[1], Baihong PAN[1], Chenglong YIN[1,4]

1 School of Biological Sciences, Center for Earth Observation and Modeling, University of Oklahoma, Norman, OK 73019, USA
2 College of Geography and Remote Sensing, Hohai University, Nanjing 211100, China
3 College of Grassland Science and Technology, China Agricultural University, Beijing 100093, China
4 School of Geographic Sciences, East China Normal University, Shanghai 200241, China

Abstract Accurate forest cover maps are the basis for estimating forest biomass and are crucial for climate regulation and biodiversity conservation, especially in sub-humid and semi-arid regions such as Oklahoma, USA. To date, there is very limited data and knowledge of the spatial pattern and temporal dynamics of forest cover in Oklahoma, and current forest cover maps have large uncertainties. In this study, multi-sensor datasets, including the Phased Arrayed L-band Synthetic Aperture Radar (PALSAR-2), Landsat, and spaceborne Light Detection and Ranging (LiDAR), were combined to generate annual forest cover maps for the years 2015 to 2021. Specifically, both PALSAR-derived HV, HH-HV, and HH/HV and Landsat-derived Normalized Difference Vegetation Index (NDVI) were used together to generate annual maps of forest cover and three forest types (evergreen, deciduous, and mixed forest) at 30-m spatial resolution for each year. The canopy height and canopy coverage samples from the Global Ecosystem Dynamics Investigation (GEDI) and the Ice, Cloud, and land Elevation Satellite-2 (ICESat-2) were used to assess forest cover maps. We also compared the spatial distribution and forested area of several forest products. Our results show that using the forest definition (canopy height > 5 m, canopy coverage > 10% over an area of 0.5 ha) of the Food and Agriculture Organization of the United Nations (FAO), the accuracy of resultant PALSAR/Landsat forest cover map for 2019 were 77.4% (GEDI) and 95.6% (ICESat-2). The estimated forested area (51,916 km^2) was moderately higher (7.2%) than the forested area from the USDA Forest Inventory and Analysis (FIA) statistics dataset (48,202 km^2) in 2017. Between 2016 and 2020, Oklahoma's forested area increased slightly by 1.9%. The PALSAR/Landsat forest maps are more accurate in western Oklahoma compared to other satellite-based forest products. The resultant annual maps of forest cover and three different forest types over Oklahoma can be used to support statewide forest management and conservation.

Keywords forest cover, evergreen forest, knowledge-based, phenology-based, land cover change

1 Introduction

Forests provide substantial ecosystem benefits and services (Felipe-Lucia et al., 2020), including preventing land degradation, regulating climate, and conserving biodiversity, particularly in semi-humid and semi-arid areas such as the state of Oklahoma, USA. According to the forest inventory conducted by Oklahoma Forestry Services (OFS) in 2016, Oklahoma's total forested area was estimated to be 49,284 km^2 (Dooley, 2017). However, forest extent varied over years due to various disturbances, such as deforestation, commercial logging, severe droughts, extreme heat, wildfires, and tornadoes. Concurrently, widespread woody plant encroachment (WPE), predominantly characterized by eastern redcedar and other juniper species into grassland areas, has occurred extensively in Oklahoma due to human activities and climate variabilities (Yang et al., 2024). To date, the spatial pattern and temporal dynamics of forest cover are still poorly understood and have significant uncertainties (Kaur et al., 2020; Adhikari et al., 2021). Thus, it is imperative to develop improved annual forest cover

Received April 29, 2024; accepted January 14, 2025

E-mail: xiangming.xiao@ou.edu

maps, which could be used to investigate the inter-annual forest area changes, thereby contributing to sustainable resource management and land use planning and policy.

Spaceborne remote sensing has been substantially applied to forest mapping and monitoring by offering frequent and large-scale observations (Luo et al., 2019; Ahmad et al., 2021; Ma et al., 2023). Optical images at high spatial resolutions (tens of meters) characterize more detailed spatial distribution and temporal dynamics of forests, which contributes critically to monitoring forest area loss, gain, and disturbances (Lu et al., 2022). Time-series Landsat images were used for deriving several current forest products. However, the accuracy of these remote sensing forest products is critically affected by clouds and aerosols and the misclassification of other vegetation types (e.g., shrubs and crops) as forests due to their similar phenological patterns and greenness characteristics (Reiche et al., 2018).

Active microwave remote sensing is also a potential solution for reliable and frequent forest mapping and monitoring due to its weather independence. The X- and C-band synthetic aperture radar (SAR) typically exhibits limited sensitivity to spatial-temporal forest variations due to the saturation of backscatter at forest canopy (mostly leaves) (Quegan et al., 2000). In comparison, the L- and P-band SAR penetrates deeper into tree crown and interacts with branches and trunks, causing substantial volume scattering (El Moussawi et al., 2019; Xu et al., 2023). However, the forest maps derived from L-band SAR data tend to include some commission errors (Shimada et al., 2014; Qin et al., 2017), particularly from other high backscatter coefficient features, such as buildings and rocky areas.

The fusion of microwave (e.g., SAR) and optical (e.g., Landsat) images products could improve forest cover maps due to their complementary strengths (Kulkarni and Rege, 2020; Shakya et al., 2022; Wang et al., 2024). Specifically, the backscatter signal of the L-band SAR from forest vegetation is higher than other cover types (e.g., grasslands, water bodies, and bare soil). Although rocky lands and build-in areas also have high backscatter signals, they have no or little vegetation and thus can be identified and excluded by vegetation indices derived from optical images. Based on this knowledge, previous studies have developed forest cover mapping methods that combined L-band microwave (PALSAR and PALSAR-2) and optical images (e.g., MODIS and Landsat) applied to South America (Qin et al., 2017, 2019), China (Qin et al., 2015), monsoon Asia (Qin et al., 2016a), and Australia (Qin et al., 2022). In addition, as the two most dominant forest types, both deciduous and evergreen forests are crucial in maintaining biodiversity, productivity, and carbon sequestration. Previous studies have explored phenology-based methods for evergreen and deciduous forests mapping in the pan-tropics (Xiao et al., 2009) and Brazilian Amazon (Sheldon et al., 2012) using PALSAR and time-series MODIS images. Historical encroachment of juniper evergreen forest maps into grasslands was generated using a pixel and phenology-based algorithm through PALSAR and time-series Landsat images in Oklahoma from 1984 to 2010 (Wang et al., 2018). Therefore, the integration of PALSAR/Landsat images and the phenology-based algorithm has the potential and capability to improve annual maps of forests, evergreen, deciduous, and mixed forests.

Accuracy evaluation of forest cover data products using sample data is a crucial component of forest mapping (Stehman and Foody, 2019; Zhang et al., 2020; García et al., 2023). In situ samples are acquired through labor-intensive, time-consuming ground surveys (Qin et al., 2016b), forest survey and inventory data (Tinkham et al., 2018), and geo-reference field photos (Xiao et al., 2011). Image-based samples (area of interest) are typically collected from very high spatial resolution (VHSR, meters) images (Gong et al., 2013), which are primarily associated with forest canopy coverage but contain limited information on canopy height. LiDAR remote sensing is widely used to precisely measure three-dimensional forest structural parameters (Duncanson et al., 2020; Potapov et al., 2021). Available spaceborne LiDAR, such as GEDI and ICESat-2, could provide a large number of highly accurate samples to characterize forest structure (e.g., canopy height, canopy profile, and canopy coverage) (Liu et al., 2021). In contrast to traditional accuracy assessment methods, LiDAR samples are densely and evenly distributed over the area of interest, universal, easily accessible, and free from subjectivity. To date, few studies have applied spaceborne LiDAR samples to evaluate the accuracy of forest cover maps.

In this study, we used three remote sensing datasets to estimate forest spatial cover based on identification of leaf and canopy, tree branches and trunk, and tree heights. The developed forest mapping algorithms are built upon the knowledge of 1) how L-band microwave data interact with tree branches and trunk, 2) how optical data interact with leaf and canopy, and 3) how LiDAR data interact with tree height and canopy profile. We combined PALSAR-2, Landsat, and LiDAR data sets to produce annual forest cover datasets (namely PALSAR/Landsat forest) in Oklahoma, a transitional region with diverse landscapes and climates. The specific objectives were 1) to generate annual maps of forest cover and evergreen, deciduous, and mixed forest from 2015 to 2021; 2) to assess the uncertainties and accuracies of the resultant forest cover maps by using samples with canopy height and canopy coverage from GEDI and ICESat-2 and comparing them with other forest cover products in Oklahoma; and 3) to analyze spatial patterns and temporal changes of forest cover during 2016−2020 across pixel, county, and state scales.

2 Materials and methods

We followed the FAO's forest definition (land at least 0.5 ha in size with a tree canopy cover of at least 10% and trees that are at least 5 m) in this study. The overall workflow included three major components (Fig. 1). First, we generated annual PALSAR/Landsat forest cover maps from 2015 to 2021 by using a knowledge-based algorithm and integrating Landsat and PALSAR-2 images. Based on the forest cover maps, we then generated evergreen, deciduous, and mixed forest maps by applying phenology-based thresholds (evergreen forest vs deciduous forest) to time-series Landsat images. Second, we conducted accuracy assessments using canopy height and coverage samples derived from ICESat-2 and GEDI and compared the spatial distribution and forest area between our forest cover maps and several other forest datasets. Third, we calculated the gross and net changes in inter-annual forest areas in Oklahoma from 2016 to 2020.

2.1 Study area

The state of Oklahoma (33.4°N–37.1°N, 94.0°W–103.2°W, Fig. 2) is located in the south-central USA and is a part of the Southern Great Plains region. It has a total area of 181,040 km^2 and consists of 77 counties. Based on the Köppen climate classification, the climate ranges from semi-arid in the west to humid subtropical in the east, characterized by large geographical and seasonal variability in both precipitation and air temperature. The elevation increases from east to west and ranges from 88 m to 1520 m above sea level. The dominant species in Oklahoma's forest include oaks, elms, pecan, eastern redcedar, and pine (Dooley, 2017).

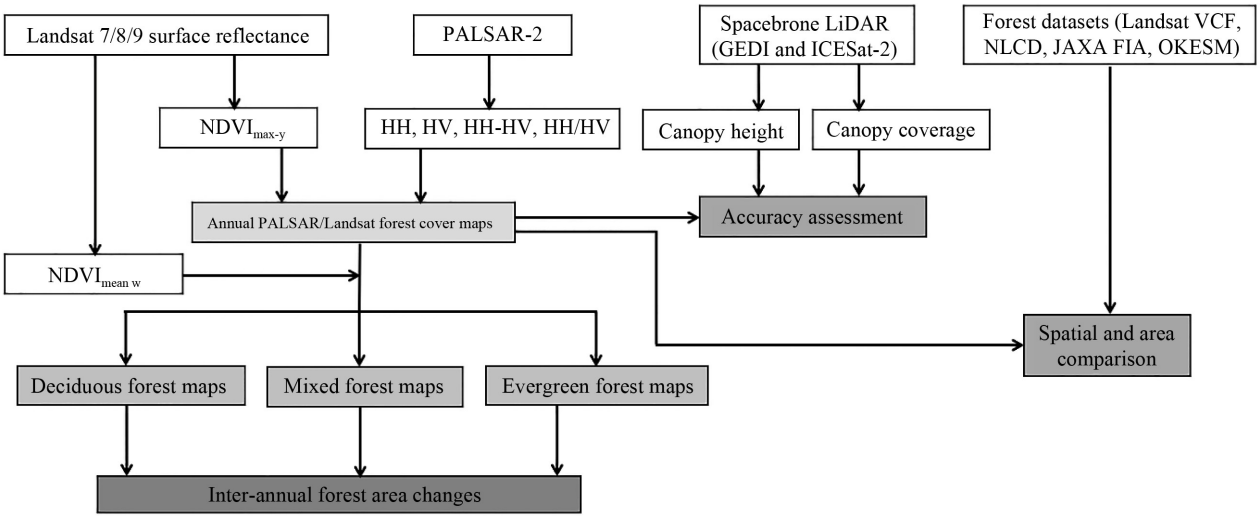

Fig. 1 The overall workflow of forest cover mapping using Landsat and PALSAR-2 images.

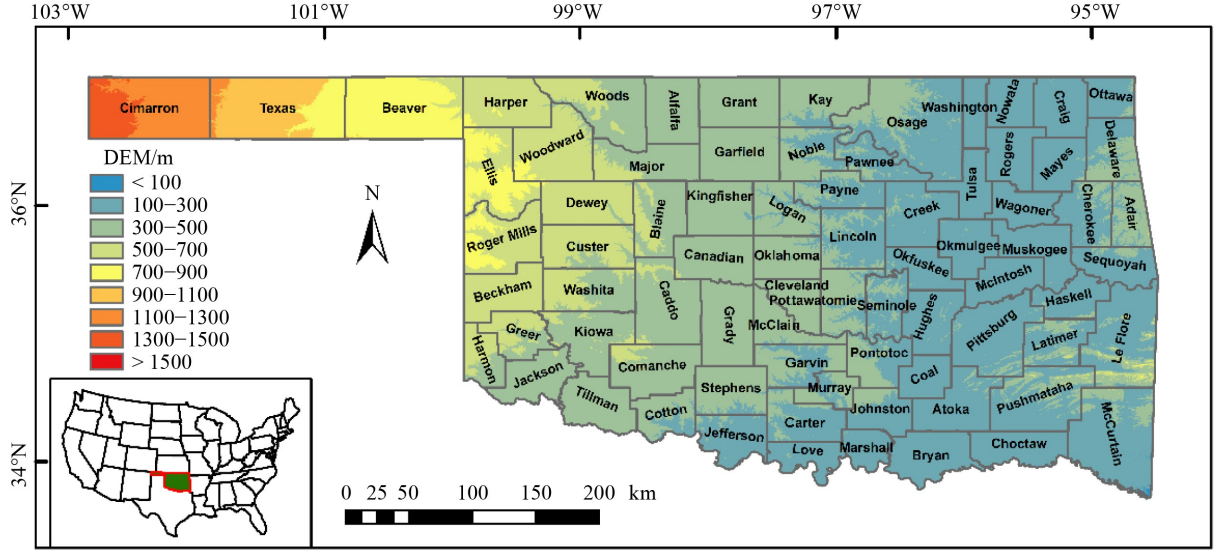

Fig. 2 The Spatial distribution of Oklahoma and its counties based on SRTM DEM.

2.2 Dataset

2.2.1 PALSAR-2 images and pre-processing

The annual Advanced Land Observation Satellite (ALOS-2) PALSAR-2 mosaics (version 2) images at 25-m spatial resolution from 2015 to 2021 were offered by the Earth Observation Research Center, Japan Aerospace Exploration Agency (JAXA) (Shimada et al., 2014). The HH and HV polarization data were ortho-rectified and slope-corrected on the Google Earth Engine (GEE) platform. The Digital numbers (DN) values of HH and HV images were converted into gamma-naught backscattering coefficients (γ^0) in decibel units. Then, the difference and ratio values of HH and HV were calculated for forest cover mapping based on Eqs. (1) and 2, where CF is the calibration factor of −83 (dB), and γ^0_{HH} and γ^0_{HV} are the corresponding backscattering coefficients:

$$\gamma^0 = 10 \times \log_{10} < DN^2 > + CF, \quad (1)$$

$$\begin{cases} \text{Difference} = \gamma^0_{HH} - \gamma^0_{HV} \\ \text{Ratio} = \gamma^0_{HH} / \gamma^0_{HV} \end{cases}. \quad (2)$$

Most PALSAR-2 images in the annual mosaics were acquired in September, October, and November each year (Fig. 3). Approximately 16% and 11% of pixels had missing PALSAR-2 data in 2016 and 2021, respectively. We analyzed the PALSAR-2 images from adjacent years and used them to gap-fill in missing data areas for the target years. We first examined PALSAR-2 data covering the missing data area in 2015 and 2017 and then calculated the average values of the PALSAR-2 backscattering coefficient images in 2015 and 2017 as the values for the missing data area in 2016. The PALSAR-2 image in 2020 was utilized to fill the missing data area in 2021.

2.2.2 Landsat images and pre-processing

The land surface reflectance (SR) of time-series Landsat 7/8/9 datasets from 2015 to 2021 is available on the GEE platform. The bad-quality observations affected by snow/ice, cloud, and cloud shadows were identified and filtered out using the quality band (pixel_qa). Approximately 90% of the pixels had more than 20 good-quality observations (Gobs) in each year from 2015 to 2021 (Fig. 4). All Gobs in the Landsat dataset were utilized to compute the Normalized Difference Vegetation Index (NDVI, Eq. (3)), where NIR and R are the SR values in near-infrared and red bands, respectively, and is used as an indicator of vegetation coverage and leaf area index. We then generated the maximum NDVI image ($NDVI_{max\text{-}y}$) through the year and the average NDVI image ($NDVI_{mean\text{-}w}$) in winter (December, January, and February) each year from Landsat images available from 2015 to 2021. $NDVI_{max\text{-}y}$ helps identify whether a pixel is covered by green vegetation and $NDVI_{mean\text{-}w}$ helps identify whether a pixel is covered by evergreen vegetation in winter.

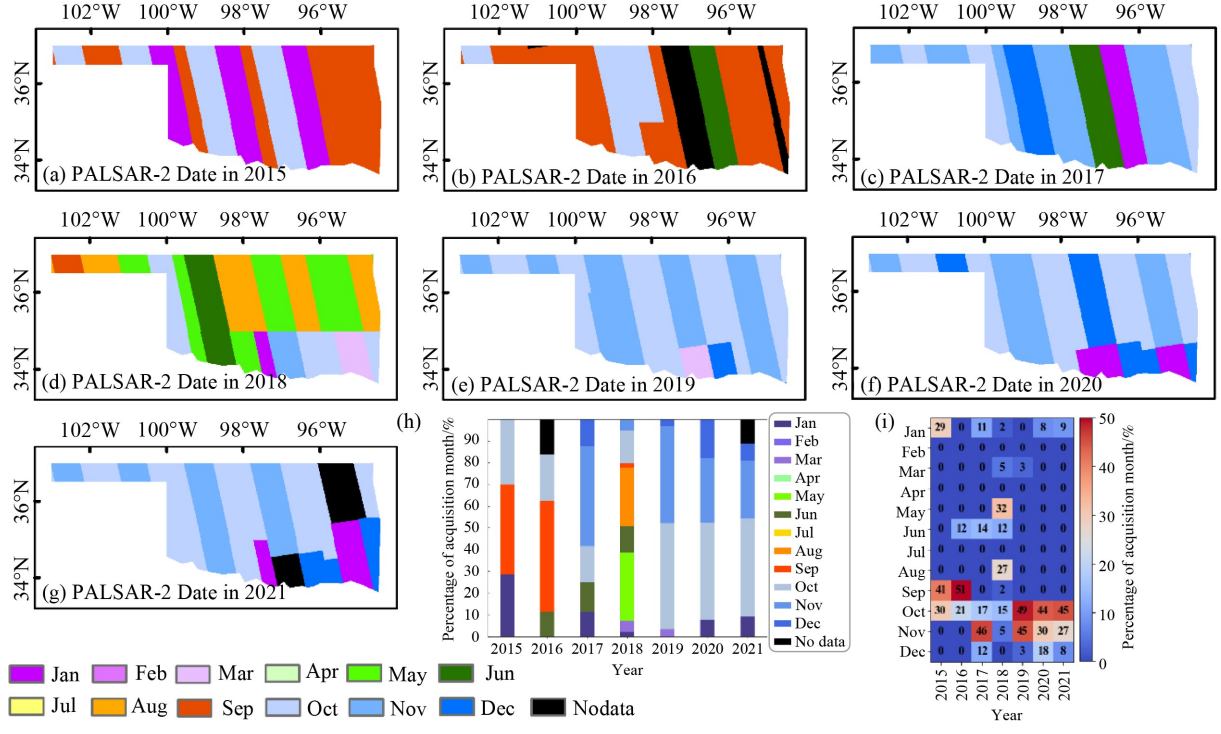

Fig. 3 Spatial distributions (a–g) of PALSAR-2 acquisition date from 2015 to 2021, and (h) the frequency (including missing data) and (i) percentage of each observation month.

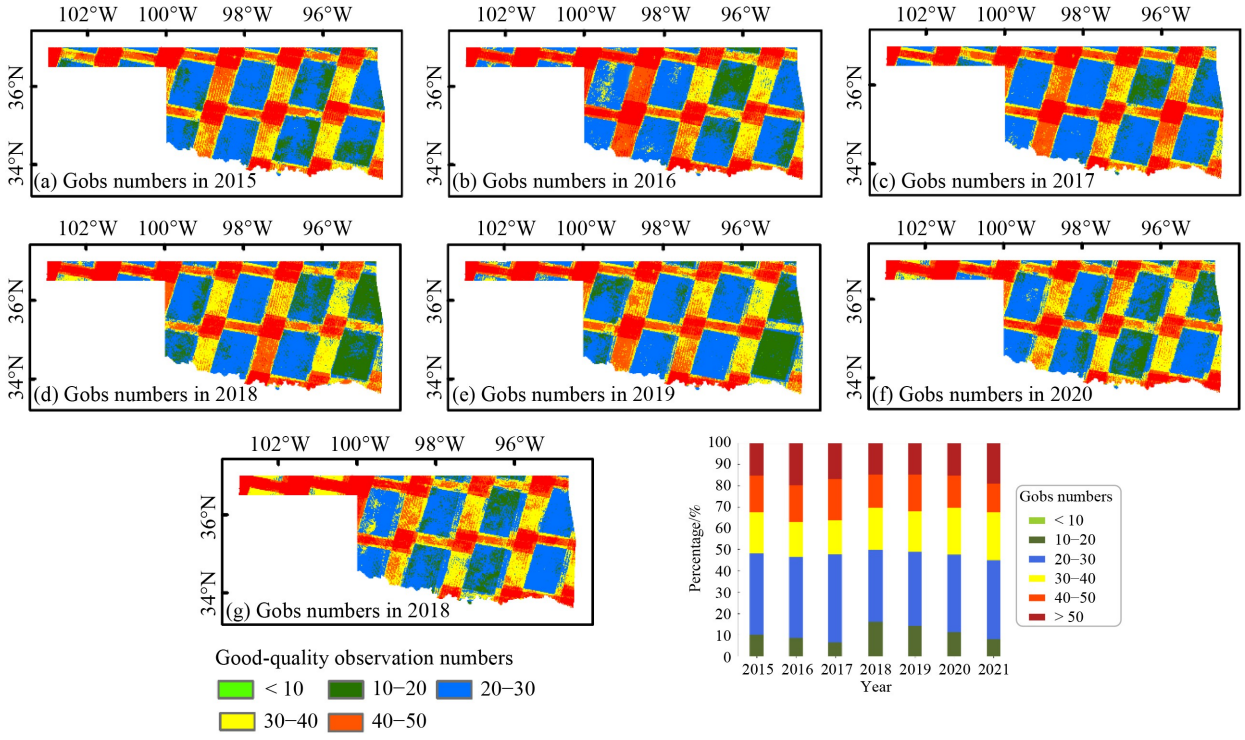

Fig. 4 Spatial distribution (a–g) and frequency (h) of Gob numbers for individual pixels over Oklahoma of all Landsat images in a year from 2015 to 2021, respectively.

$$\mathrm{NDVI} = \frac{NIR - R}{NIR + R}. \quad (3)$$

2.2.3 Accuracy assessment sampling data from Spaceborne LiDAR products

2.2.3.1 GEDI footprint samples

The GEDI mission is designed to characterize the dynamic and structure of forest ecosystems to understand the Earth's carbon and biodiversity. The GEDI Level 2A Geolocated Elevation and Height Metrics Product (GEDI02_A) provides height information for ground and canopy (Dubayah et al., 2021a). The GEDI Level 2B Canopy Cover and Vertical Profile Metrics product (GEDI02_B) offers multiple biophysical metrics, such as canopy coverage and plant area-related datasets (Dubayah et al., 2021b). We downloaded the GEDI02_A and GEDI02_B products covering Oklahoma for 2019 and 2020 for evaluating forest maps for 2019 and 2020, respectively. We then selected the GEDI footprints from a Coverage beam (id: 0000) and another Full power beam (id: 0110) separated by 3 km, with a sampling interval of 1.2 km along the track. The relative height metrics at 98% (RH98) from GEDI02A and canopy cover from GEDI02_B were used to construct GEDI samples for accuracy assessment of forest maps. There were 63,990 and 94,061 GEDI samples in 2019 and 2020, respectively. In 2019, 17,977 samples (28%) covering Oklahoma met the FAO forest definition (Figs. 5(a)–5(c)), and the remaining 46013 samples (72%) did not meet the FAO forest definition, primarily located in central and western Oklahoma.

2.2.3.2 ICESat-2 ATL08 samples

The Advanced Topographic Laser Altimeter System (ATLAS) instrument utilizes photon-counting technology and generates six beams arranged in three pairs for altimetry observations (Neuenschwander and Pitts, 2019). The ATLAS/ICESat-2 L3A Land and Vegetation Height product (ATL08) provides along-track terrain height, canopy height, and canopy cover in fixed 100-m segments (Neuenschwander and Pitts, 2019). We downloaded the ATL08 product covering Oklahoma for the years 2018 to 2020 to evaluate forest maps, respectively. We selected the ICESat-2 segments from the strong beams of each track pair (3 km apart) with an equal sampling interval of 1.2 km along the track to make it consistent with the sampling interval of GEDI samples. The canopy height and canopy coverage of ATL08 segments were used to form ICESat-2 samples, together with GEDI samples, for subsequent forest map evaluation. There were 7129, 35156, and 39838 ICESat-2 samples in 2018, 2019, and 2020, respectively. In 2019, 27543 samples (78%) covering Oklahoma met the FAO forest definition (Figs. 5(d)–5(f)), and the remaining 7613 samples (22%) did not meet the FAO forest definition, mostly located in western Oklahoma.

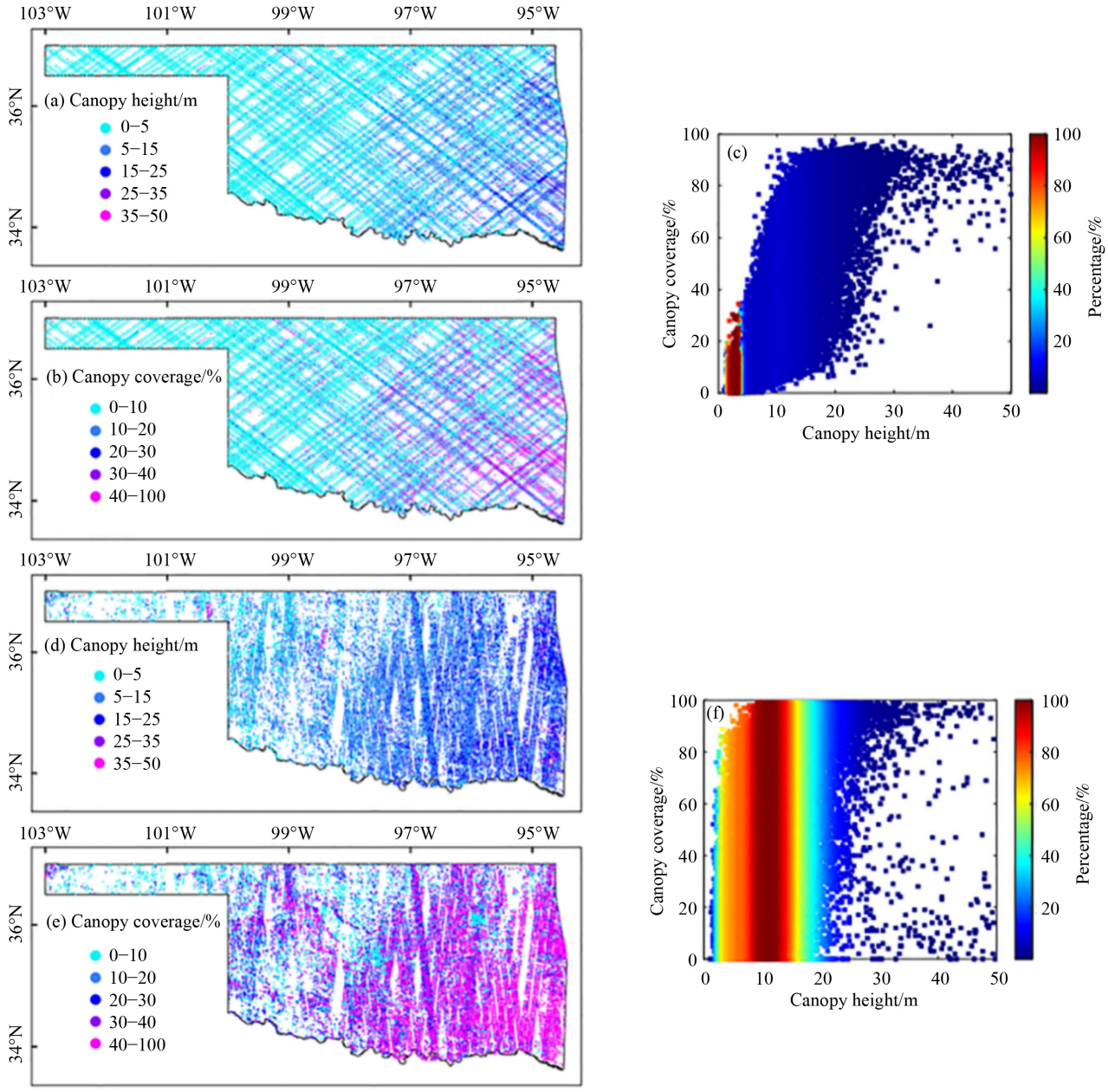

Fig. 5 Spaceborne LiDAR samples over Oklahoma in 2019, including spatial distribution and the histogram of canopy height (m) and canopy coverage (%) for (a–c) GEDI footprint samples and for (d–f) ICESat-2 ATL08 samples.

2.2.4 Other forest cover data products and pre-processing

We used a total of seven additional forest cover products to further assess the generated forest maps from this study (Table 1): two SAR-based forest products from JAXA; two optical-based forest products, the National Land Cover Database (NLCD 2019) and the Landsat Vegetation Continuous Fields tree cover dataset (Landsat-VCF); a statewide forest product from the Oklahoma Ecological Systems classification and mapping project (OKESM); and USDA forest inventory and Analysis (FIA). Forest spatial distribution over Oklahoma from the five satellite-based forest products can be seen in Fig. 6.

2.2.4.1 Global JAXA FNF products

The annual global JAXA FNF datasets were generated by classifying 25-m L-band PALSAR/PALSAR-2 image mosaic data using region-specific threshold values during 2007–2010 and 2015–2017 (Shimada et al., 2014). In addition, JAXA provided a new version of global FNF datasets (JAXA FNF v2) during 2017–2020 generated from ALOS-2 PALSAR-2 image mosaic using the random forest method. The JAXA FNF v2 included four land types: “dense forest” (canopy cover of 90% or more), “non-dense forest” (canopy cover of 10% to less than 90%), non-forest, and water. The forest definition

Table 1 Characteristics of multiple forest cover products

Dataset	Forest definition		Major data source	Methods	Spatial resolutions	Periods
	Canopy height	Canopy cover				
FIA	> 5 m	> 10%	Inventory	Plot sampling and statistics	state	Annual sampling design after 1998
OKESM	> 4 m	> 25%	Landsat and aerial images	Decision tree	10 m	2015
Landsat-VCF	> 5 m		MODIS-VCF and Landsat 5/7	Decision tree	30 m	2000, 2005, 2010, 2015
NLCD	> 5 m	> 20%	Landsat 5/7	Decision tree	30 m	Circa 2001, 2004, 2006, 2008, 2011, 2013, 2016, 2019, and 2021
JAXA	> 5 m	> 10%	PALSAR, PALSAR-2	Rule-based	25 m	2007–2010, 2015–2017
JAXA v2	> 5 m	> 10%	PALSAR-2	Decision tree	25 m	2017–2020
PALSAR/Landsat	> 5 m	> 10%	PALSAR-2 and Landsat	Rule-based	30 m	2015–2021

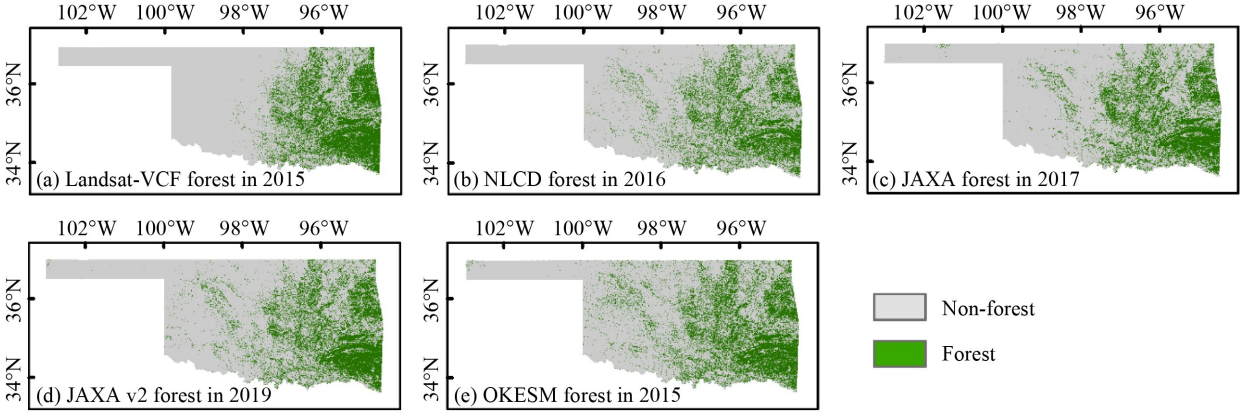

Fig. 6 Spatial distribution of five satellite forest products over Oklahoma including (a) Landsat-VCF in 2015; (b) NLCD in 2016; (c) JAXA in 2017; (d) JAXA v2 map in 2019; (e) OKESM in 2015.

for JAXA FNF aligns with the FAO forest definition. We merged JAXA FNF v2 "dense forest" and "non-dense forest" into the "forest" class.

2.2.4.2 NLCD 2019 forest products

The NLCD 2019 product offers land cover data of the United States using the Anderson Level II classification system and 30-m Landsat images. The forest definition for NLCD is canopy height > 5 m and canopy coverage > 20%. The NLCD 2019 product (available at MRLC website) has 28 different land cover types for 2001, 2004, 2006, 2008, 2011, 2013, 2016, and 2019 (Homer et al., 2020). We merged the NLCD classes of "deciduous forest," "evergreen forest," and "mixed forest" into the "forest" class.

2.2.4.3 Landsat-VCF forest products

The Landsat-VCF dataset (available at LCLUC website) provides estimates of the proportion of tree cover within 30-m pixels, encompassing woody vegetation exceeding 5-m in height and derived from Landsat 5/7 images (Sexton et al., 2013). The Landsat-VCF dataset is available in 2000, 2005, 2010, and 2015. We designated pixels with tree cover exceeding 10% as forested areas for Landsat-VCF product in 2015.

2.2.4.4 OKESM forest dataset

The 10-m OKESM dataset (available at Wildlifedepartment.Com website) was funded by the Oklahoma Department of Wildlife Conservation (ODWC) and Great Plains Landscape Conservation Cooperatives (LCCs) and completed between 2012 and 2015 (Diamond and Elliott, 2015). The forest definition for OKESM is tree canopy coverage > 25% and canopy height > 4 m. The OKESM map incorporated remote sensing for land cover (approximately 15 classes) and overlaid digital soils, slopes, and streams to generate the 165 land cover types classification map in 2015. Subsequently, we divided forest and woodland categories (including Post Oak, Eastern Redcedar, Blackjack Oak, Ashe juniper, and mixed forest, etc.) as "forest" , and the rest were divided into "non-forest".

2.2.4.5 FIA inventory data

The FIA dataset includes forest resource statistics (e.g., forest area, diversity, biomass, volume, mortality, and

removals) at state, regional, and national scales released by the USDA Forest Service (available at USDA website) (Hoover et al., 2020). The forest definition for FIA data is consistent with the FAO. We used the forest area estimate of Oklahoma in 2017 to compare it with other satellite-based forest products.

Among these forest products, we selected the JAXA FNF maps from 2015 to 2017, JAXA FNF v2 maps from 2017 to 2020, NLCD 2019 map, Landsat-VCF map in 2015, and OKESM in 2015 for comparison (Fig. 6). All datasets were re-projected into the "USA_Contiguous_Albers_Equal_Area_Conic" coordinate system using the nearest neighbor method. Subsequently, the total forested area for Oklahoma was calculated from each dataset.

2.3 Forest cover mapping methods2.3.1 PALSAR/Landsat forest cover mapping algorithm

Forests typically exhibit a higher leaf area index (LAI) compared to rocky lands, barren lands, and built-up surfaces with minimal or no green vegetation throughout the year. We used the approaches developed in previous studies to identify and generate annual maps of forest cover in Oklahoma (Qin et al., 2016b; Wang et al., 2024). The decision rules for forests were determined by using both structure/biomass-sensitive data (HV, HH-HV, and HH/HV) and vegetation coverage-sensitive data ($NDVI_{max\text{-}y}$). Based on the PALSAR and Landsat NDVI threshold values trained by ground reference data in the United States of America, Hainan island of China, and monsoon Asia in our previous studies, forest pixels were identified by defining specific pixel value ranges: $-19 \leqslant HV \leqslant -7.5$, $0 \leqslant HH\text{-}HV \leqslant 9.5$, and $0.2 \leqslant HH/HV \leqslant 0.95$ (Qin et al., 2016a; Chen et al., 2018; Wang et al., 2024) and $NDVI_{max\text{-}y} \geqslant 0.7$ (Qin et al., 2016b) to eliminate commission errors in PALSAR-2-based forest maps and generate the PALSAR/Landsat forest maps (Qin et al., 2016b). In this process, we used the nearest neighbor method to resample the 25-m PALSAR-2-based forest maps to 30-m and generate the resultant annual PALSAR/Landsat forest cover maps from 2015 to 2021.

To reduce forest classification uncertainty, we utilized a three-year moving window filter to examine temporal and logical consistency in the series of forest cover maps from 2015 to 2021. The reasonable sequences of forest/non-forest in continuous three years were FFF, FFN, FNN, NFF, NNF, and NNN, where F indicated forest and N indicated non-forest. However, NFN and FNF were considered "not reasonable sequences" as forests cannot suddenly appear and disappear in year-to-year dynamics, and we modified them as NNN and FFF, respectively. This post-processing step could not be implemented for the first year (2015) and the last year (2021), thus we calculated the annual forest map statistics from 2016 to 2020, which had higher confidence than forest maps in 2015 and 2021.

2.3.2 Evergreen, deciduous, and mixed forest mapping algorithms

Evergreen forests maintain their green leaves throughout the entire year, whereas deciduous trees change in leaf color and shed them during winter due to low air temperatures. The differences in leaf phenology between evergreen forests and other forest types can be effectively captured by time series vegetation indices, such as NDVI, Enhanced Vegetation Index (EVI), and Land Surface Water Index (LSWI). Seasonal characteristics of NDVI were analyzed for training samples of evergreen forest and other forest types. The average value of NDVI ($NDVI_{mean\text{-}w}$) in winter was particularly effective in separating evergreen forests from deciduous and other forest types. Within all forested pixels, we used thresholds of $NDVI_{mean\text{-}w} \geqslant 0.4$ and $NDVI_{mean\text{-}w} < 0.3$ to identify evergreen and deciduous forest pixels, respectively (Wang et al., 2018). The remaining pixels were classified as mixed forests. Subsequently, the temporal and logical consistency checks (3-year temporal window) were also applied to evergreen, deciduous, and mixed forest maps.

2.4 Forest map accuracy assessment by spaceborne LiDAR samples

To evaluate the accuracies and uncertainties of PALSAR/Landsat forest cover maps under the FAO forest definition, we separated the LiDAR samples located in forest cover areas and filtered out 3961 (from ICESat-2), 38232 (20333 from ICESat-2 and 17899 from GEDI), and 54714 (22664 from ICESat-2 and 32050 from GEDI) samples in PALSAR/Landsat forest cover maps for 2018 (Fig. 7(a)), 2019 (Fig. 7(b)), and 2020 (Fig. 7(c)), respectively. We then calculated the percentage of LiDAR samples meeting the FAO forest definition and generated 2D scatter plots of canopy height and canopy coverage from filtered samples to determine the resultant assessment accuracy.

2.5 Comparison of multiple forest cover datasets

To analyze the uncertainty and consistency across multiple forest datasets in Oklahoma, we aggregated all satellite-forest cover products to 150 m forest cover fractional maps using the nearest neighbor method. Then, we set the threshold value of 50% to convert them into binary forest cover maps, which were subsequently separated into two groups. Forest datasets in 2015 included our forest maps, JAXA, Landsat-VCF, and OKESM. Forest datasets in 2019 included our forest maps, NLCD, and JAXA v2. In terms of spatial distribution comparisons, we overlaid multiple forest datasets and calculated the forested pixel consistency of

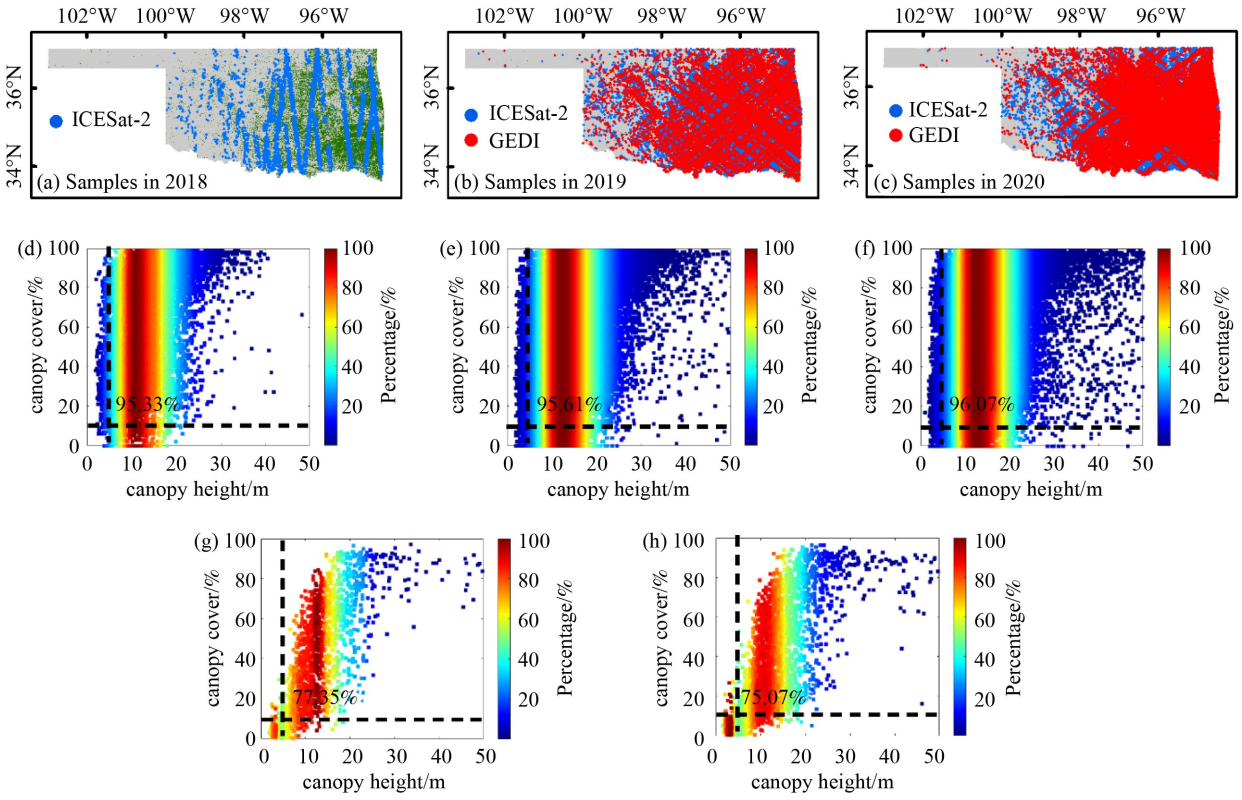

Fig. 7 Assessment accuracy of PALSAR/Landsat forest maps from 2018 to 2020. (a–c) Spatial distribution of LiDAR samples within forested areas from 2018 to 2020, respectively; the 2D scatter plots of canopy height and canopy coverage for (d–f) ICESat-2 ATL08 samples from 2018 to 2020 and (g, h) GEDI samples in 2019 and 2020.

the forest datasets for 2015 and 2019. In addition, we calculated the percentage of consistent forested pixels and forested versus non-forested pixels for inter-comparing spatial distribution between our forest maps and other forest datasets for both 2015 and 2019. In terms of the forested area comparison, we calculated and compared the forested area of our forest maps from 2015 to 2021, JAXA forest maps from 2015 to 2017, JAXA v2 forest maps from 2017 to 2020, NLCD forest maps in 2016 and 2019, Landsat-VCF forest map in 2015, OKESM map in 2015, and FIA data in 2017 at state scale. Furthermore, we calculated the forested area for each county in Oklahoma and conducted linear regression comparisons between our forest maps and other satellite-forest datasets for both 2015 and 2019.

2.6 Analyses of forest cover changes from 2016 to 2020

To quantify the spatial-temporal changes in forest cover in Oklahoma, we overlaid the forest cover maps in 2016 and 2020 and identified and quantified the spatial distribution of forest loss (transition from forest to non-forest) and gain (transition from non-forest to forest) at the pixel scale. On the state scale, we calculated annual gross gain and loss and net change in forest cover, evergreen, deciduous, and mixed forest from 2016 to 2020. In addition, we calculated the forested area for each county from 2016 and 2020.

3 Results

3.1 Accuracy assessment of annual PALSAR/Landsat forest cover maps

The accuracy of the annual forest cover maps was assessed based on the percentage of pixels meeting FAO forest definition (Table 2) and frequency distribution of LiDAR samples within the forested area (Fig. 7). Figures 7(d)–7(f), 7(g), and 7(h) show the 2D scatter plots of canopy height and canopy coverage for ICESat-2 samples from 2018 to 2020 and for GEDI samples in 2019 and 2020. The percentage of ICESat-2 samples that met either FAO forest criteria “canopy height >5 m” or “canopy coverage >10%” was approximately 97% from 2018 to 2020. The average percentage of ICESat-2 samples that met both was 95.7%. In addition, about 81.3% of GEDI samples met the criteria “canopy height >5 m,” while about 77.7% met the criteria “canopy coverage >10%” in 2019 and 2020. The average percentage of GEDI samples that met both was 76.2%. It clearly demonstrated that our forest cover maps have relatively high accuracy evaluated by both ICESat-2 and GEDI samples.

Table 2 The accuracy of PALSAR/Landsat forest maps evaluated by structural properties of GEDI and ICESat-2 samples

Year	GEDI				ICESat-2			
	Total samples	Canopy height > 5 m	Canopy coverage > 10%	Canopy height > 5 m, canopy coverage > 10%	Total samples	Canopy height > 5 m	Canopy coverage > 10%	Canopy height > 5 m, canopy coverage > 10%
2018					3,961	3,849 (97.17%)	3,883 (98.03%)	3,776 (95.33%)
2019	17,899	14,725 (82.27%)	14,102 (78.79%)	13,845 (77.35%)	20,333	19,950 (98.11%)	19,790 (97.33%)	19,441 (95.61%)
2020	32,050	25,765 (80.39%)	24,558 (76.62%)	24,061 (75.07%)	22,664	22,294 (98.37%)	22,105 (97.53%)	21,774 (96.07%)

3.2 Annual PALSAR/Landsat forest maps

3.2.1 Spatial distribution of forest cover and evergreen, deciduous, and mixed forest maps

The total, evergreen, deciduous, and mixed forest areas had distinct spatial distribution patterns in Oklahoma (Figs. 8 and 9). Most forests were concentrated in southeastern, northeastern, and central Oklahoma, while only a small area of forests was distributed in western Oklahoma (Fig. 8). The average percentage of forest and non-forest area between 2015 and 2021 was 29% and 71%. Forests in Oklahoma were dominated by evergreen and mixed forests. Evergreen forests were mainly concentrated in southeastern Oklahoma, while mixed forests were distributed in the central and northeastern Oklahoma. A smaller expanse of deciduous forests was also observed (Fig. 9). The average percentage of evergreen, deciduous, mixed, and non-forest areas between 2015 and 2021 for Oklahoma was 12.9%, 2.1%, 14.0%, and 71%, respectively.

3.2.2 Forest changes (gain or loss) at the pixel scale

From 2016 to 2020, 93.9% of classified pixels in Oklahoma remained unchanged, with 67.7% forested areas and 26.2% non-forested areas (Fig. 10). In contrast, 2.8% of pixels underwent a transition from forest to non-forest, while 3.3% of pixels experienced a shift from non-forest to forest. A large amount of forest cover has been lost in western Oklahoma (Fig. 10(b)). Noticeable forest cover gain and loss were mainly concentrated in southeastern Oklahoma (Fig. 10(c)).

3.2.3 Inter-annual changes (gain or loss) of forest areas at state and county scales

The forested area of Oklahoma increased slightly (~1.9%) from 2016 to 2020 with a minor loss of forested area between 2016 and 2017 (Figs. 11(a) and 11(b)). Evergreen forested area was 22,595 km^2 in 2016 and had no significant change during 2016–2020 (Figs. 11(a) and 11(c)). Deciduous forest area increased from 3,115 km^2 to 3,655 km^2 in 2020 (~17.3% increase) with a minor loss of deciduous forest between 2016 and 2017 (Figs. 11(a) and 11(d)). The mixed forest area consistently, but only slightly increased from 26,721 km^2 in 2016 to 27,185 km^2 in 2020 (~1.7% increase) (Figs. 11(a) and 11(e)).

From 2016 to 2020, 30-one Oklahoma counties showed an increase in forest area (Table S1, Fig. 12), mostly

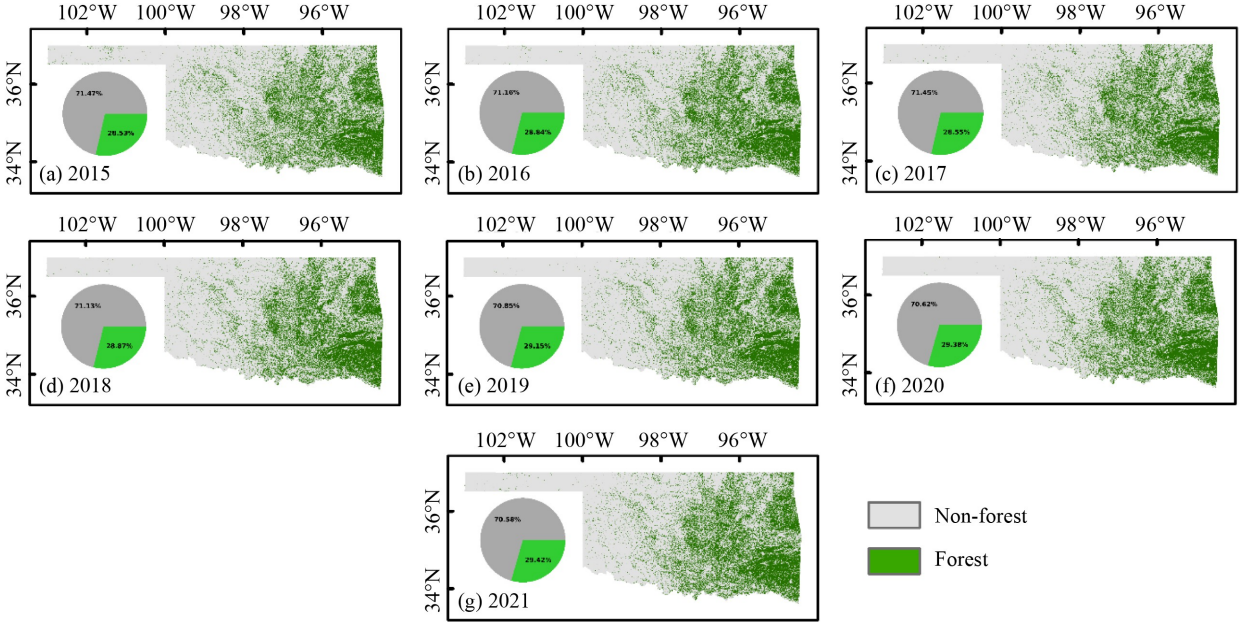

Fig. 8 Spatial distributions of annual PALSAR/Landsat forest cover maps in Oklahoma from 2015 to 2021, respectively.

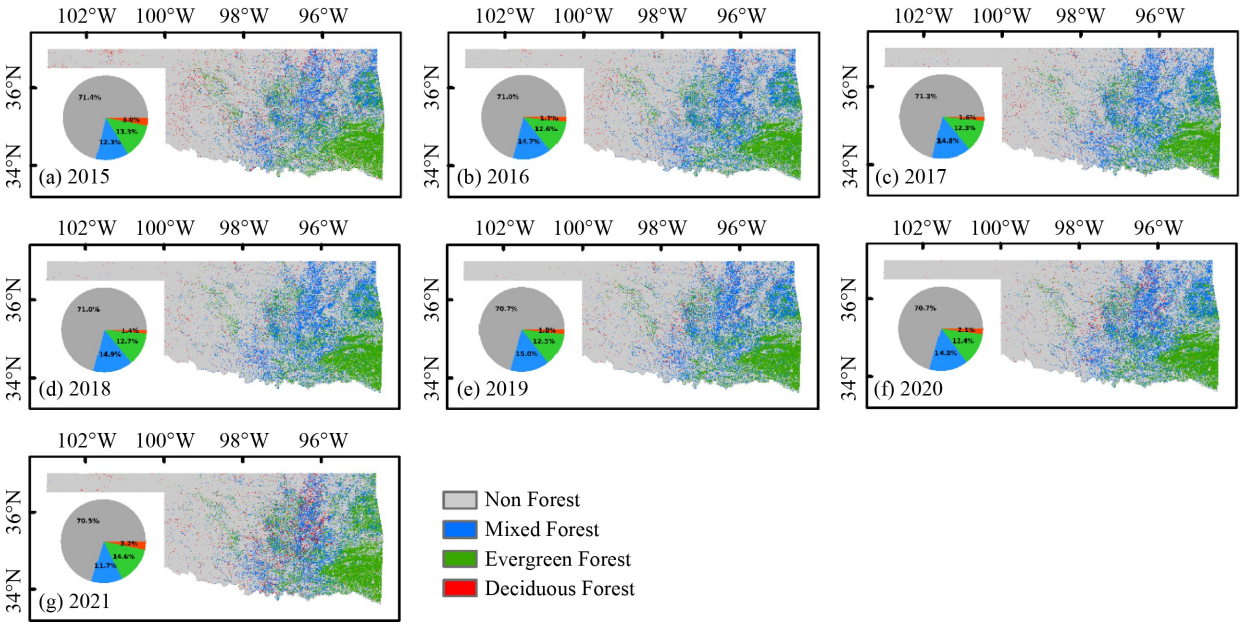

Fig. 9 Spatial distributions of annual PALSAR/Landsat evergreen, deciduous, and mixed forest maps from 2015 to 2021, respectively.

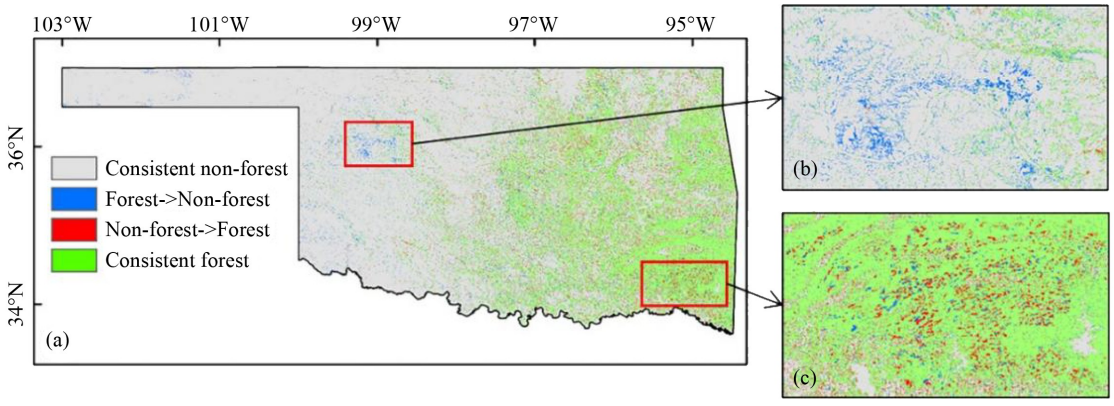

Fig. 10 Spatial distribution of forest cover changes for (a) Oklahoma from 2016 to 2020 and the zoom-in areas in (b) western Oklahoma and (c) southeastern Oklahoma.

located in regions with high forest coverage in eastern Oklahoma. Twenty counties showed a decrease in forested area, primarily in western Oklahoma with sparse forest coverage, and the remaining 26 counties in the central region had either a decrease and then an increase or no clear change trend.

3.3 Comparison of forest area estimates at state and scales

3.3.1 Comparison of forest cover map at pixel scale

The PALSAR/Landsat forest maps (Figs. 8 and 9) showed high consistency in central, northeastern, and southeastern Oklahoma and identified more forested cover areas in arid western Oklahoma than the other forest products in both 2015 and 2019 (Fig. 13). In 2015 (Fig. 13(a)), the consistency of forest pixels in all four forest maps was 46.1%, with an additional 16.0% and 14.8% consistency between 2 and 3 maps, respectively, and no consistency in 23.1% of pixels. Approximately 67.9%, 65.2%, and 71.6% of pixels were recognized as consistently forested areas when comparing our forest cover map with the OKESM forest map, JAXA forest map, and Landsat-VCF forest map, respectively (Figs. 13(c)−13(e)). Geographically, the OKESM, JAXA, and Landsat-VCF forest maps had 15.9%, 12.3%, and 7.1% more forest area, respectively, in central, northeastern, and southeastern Oklahoma, and 16.2%, 22.5%, and 21.3% less forest area, respectively, than PALSAR/Landsat forest map in western Oklahoma.

In 2019, the consistency of forest pixels in three, two, and one forest maps was 57.9%, 19.9%, and 22.2%, respectively (Fig. 13(b)). Approximately 65.5% and 72.6% of pixels were identified as consistent forested areas when comparing our forest cover map with the NLCD 2019 forest map and JAXA v2 forest map (Figs.

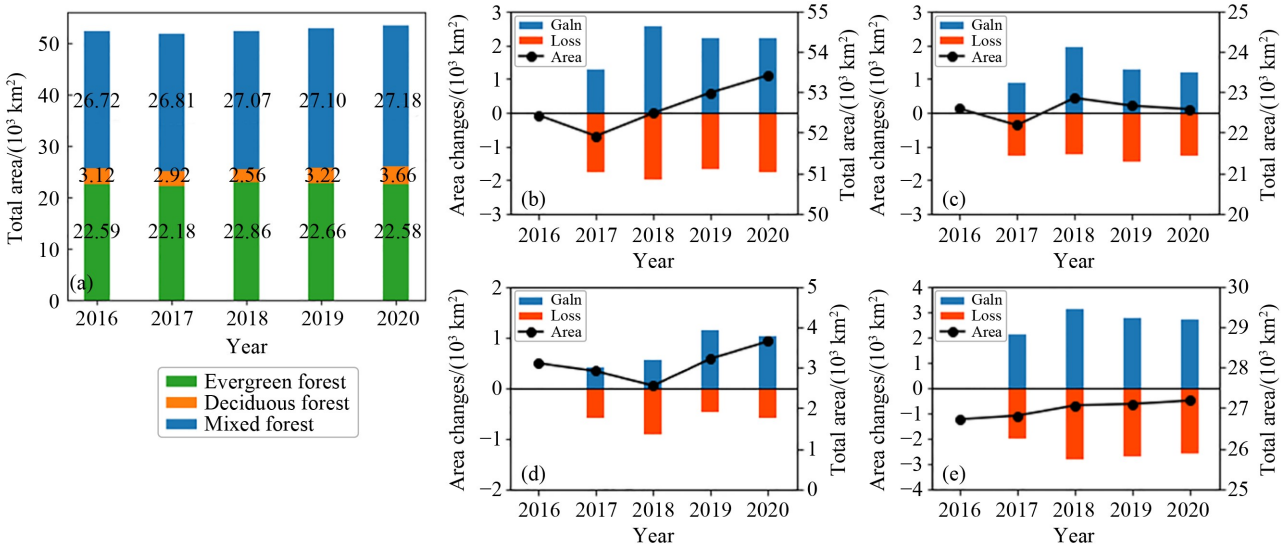

Fig. 11 Statistics of forest area changes in Oklahoma from 2016 to 2020, including (a) total area and gross gain and loss of (b) forest cover, (c) evergreen, (d) deciduous, and (e) mixed forest.

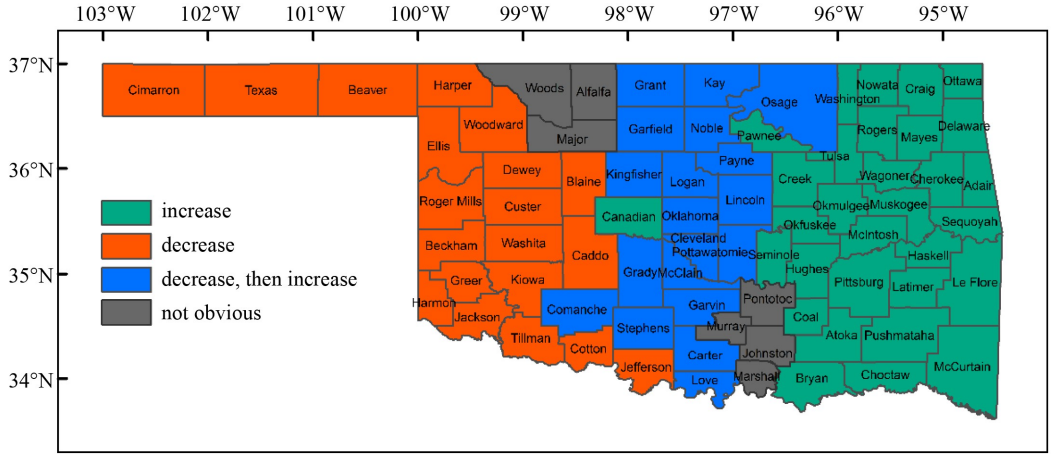

Fig. 12 Trends in forested area for each county from 2016 to 2020.

13(f) and 13(g)), respectively. Geographically, the NLCD 2019 and JAXA FNF v2 forest maps had 6.0% and 5.8% more forested area, respectively, in central, northeastern, and southeastern Oklahoma, and 28.5% and 21.6% less forested area, respectively, in western Oklahoma than the PALSAR/Landsat forest cover map. This comparison indicates our forest cover map and the other forest cover maps had relatively high spatial distribution consistency in central, southeastern, and northeastern Oklahoma and large uncertainty in western Oklahoma.

3.3.2 Comparison of forest area estimates at state and county scales

The PALSAR/Landsat forested area in 2015 (51,852 km^2) was close to OKESM forest map (50,302 km^2) (Fig. 14, Table 3). The forest area from the forest cover map of this study in 2017 (51,916 km^2) was moderately higher (7.2%) than FIA statistics data (48,202 km^2) and substantially higher than JAXA FNF forest map (43,814 km^2) and JAXA v2 forest map (41,838 km^2) in 2017. The forest area of PALSAR/Landsat forest map in 2019 (52,990 km^2) was substantially higher than NLCD 2019 forest map (40,216 km^2).

The forest area estimates for 77 Oklahoma counties in both 2015 and 2019 had significant linear relationships ($R^2 > 0.95$) between the PALSAR/Landsat forest cover map and the other forest datasets (Fig. 15). The forest area of counties in OKESM map tended to be slightly higher, while JAXA forest map tended to have lower forest areas than forest area estimated from the forest cover map of this study in 2015. The forest area for counties in Landsat-VCF forest map was obviously lower than forest cover map of this study in 2015 (Fig. 15(a)). In addition, the forest area of counties in JAXA FNF v2 map and NLCD 2019 forest map tended to have lower forest areas than PALSAR/Landsat forest map in 2019 (Fig. 15(b)).

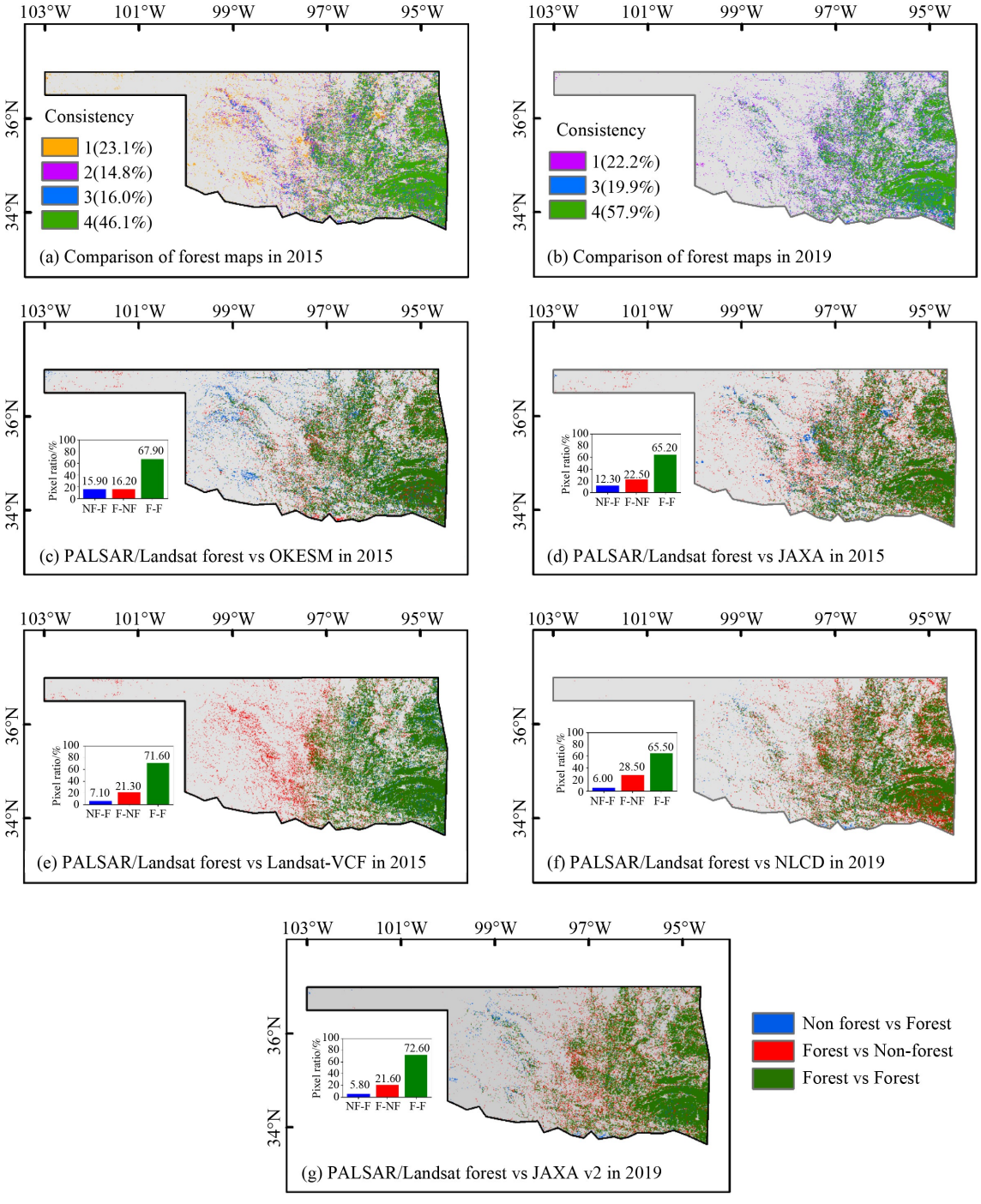

Fig. 13 Overall spatial distribution comparison of forested pixels among forest cover maps in (a) 2015 and (b) 2019 and inter-comparison between PALSAR/Landsat forest maps and (c) OKESM, (d) JAXA, (e) Landsat-VCF, (f) NLCD, and (g) JAXA v2 map.

4 Discussion

4.1 The integration of PALSAR-2, Landsat, and LiDAR datasets

This study integrated optical data from Landsat, microwave data from PALSAR-2, and LiDAR data from GEDI and ICESat-2 to generate and evaluate annual forest cover and forest cover type maps for Oklahoma. The leaf/canopy phenological characteristics between evergreen and deciduous forests can be effectively distinguished based on $NDVI_{mean\text{-}w}$ (Wang et al., 2017). However, owing to the limited numbers of high-quality observations of Landsat datasets for three months in winter and the missing strips in Landsat 7, small areas could not be fully covered by good-quality observations from Landsat 7/8/9, leading to uncertainties in spatial distribution and area estimates of evergreen, deciduous,

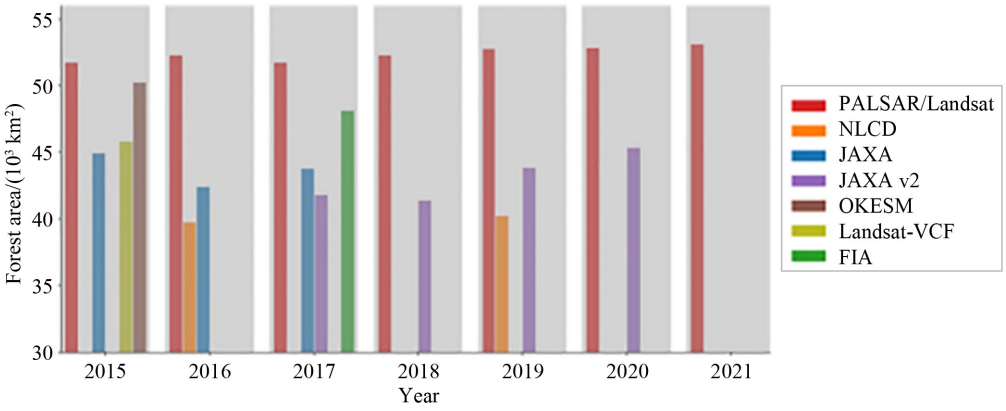

Fig. 14 Comparison of the forested area estimates for Oklahoma among multiple forest datasets, including PALSAR/Landsat forest maps from 2015 to 2021, Landsat-VCF forest map in 2015, NLCD forest maps in 2016 and 2019, JAXA forest maps from 2015 to 2017, JAXA v2 forest maps from 2018 to 2020, OKESP map in 2015, and FIA data in 2017.

Table 3 Forested area statistics among multiple forest datasets

Forest area (10^3 km^2)	2015	2016	2017	2018	2019	2020	2021
PALSAR/Landsat	51.9	52.4	51.9	52.5	53.0	53.4	53.5
FIA			48.2				
OKESM	50.3						
VCF	45.6						
NLCD		39.8			40.0		
JAXA	44.7	42.1	43.6				
JAXA v2			41.6	41.2	43.7	45.2	

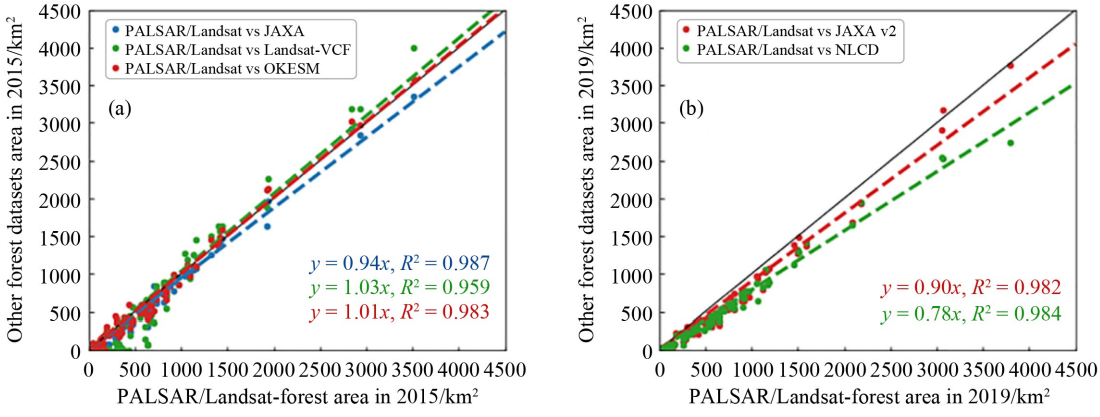

Fig. 15 Comparison of forested area of PALSAR/Landsat forest cover maps with other satellite-based forest products in (a) 2015 and (b) 2019. Each point represents an individual Oklahoma county. Colored linear regression lines represent the relationship between other satellite-based products and the PALSAR/Landsat estimate of forested area from this study. The solid black line is the 1:1 relationship.

and mixed forests, especially in 2021 (Fig. 9(g)). Furthermore, the vegetation structure-based products derived from GEDI and ICESat-2 offer a new source of samples for forest accuracy assessment (Markus et al., 2017; Patterson et al., 2019). However, the relatively large differences in accuracy and frequency distribution between GEDI and ICESat-2 (Fig. 7) may be due to the different retrieval principles for canopy height and canopy coverage and uncertainties in products. Specifically, for the forest canopy height products, GEDI generated forest height products by linearly interpolating the L1B elevations and then computing them in relation to the height of the lowest detected mode (Dubayah et al., 2021a). In contrast, the forest canopy height product of ICESat-2 was organized into a cumulative distribution, calculated by the difference between the classified canopy photons' height and the estimated terrain surface (Neuenschwander and Pitts, 2019). Numerous studies

comparing the accuracy of forest canopy height retrieval showed that GEDI was slightly more accurate than ICESat-2, especially strong power beam data have improved accuracy (Liu et al., 2021; Zhu et al., 2022; Yu et al., 2024). In addition, GEDI-derived canopy coverage was the estimation of canopy fractional cover, which characterizes the percent of the ground covered by the vertical projection of canopy component within the spot area (~25 m) under the off-nadir angle of less than 6° (Dubayah et al., 2021b). In contrast, the average canopy cover value for the ICESat-2 segment was computed from the external Landsat-VCF product (Sexton et al., 2013; Neuenschwander and Pitts, 2019).

4.2 Comparison between PALSAR/Landsat forest map and the other forest products

Compared to the other forest cover products, the PALSAR/Landsat forest cover maps have several advantages. First, in terms of input data sources, this study used a combination of complementary PALSAR-2 and Landsat images compared to other products that used only optical or SAR data (Table 1). Second, the knowledge-based approach in this study was sensitive to both woody (trunk and branches) and leafy parts and thus could robustly capture the existence of forest (tree) cover. Although other satellite-forest data products used decision tree algorithms, some required training samples from each year. Third, the PALSAR/Landsat forest cover maps were annual and spanned the temporal period 2015−2021 compared to other discontinuous forest cover products (FIA, OKESM, Landsat-VCF, and NLCD) and shorter temporal periods (JAXA and JAXA v2).

The PALSAR/Landsat forest cover maps identified significantly more forest areas than other maps in the arid region of western Oklahoma (Fig. 13), which contains relatively low forest coverage. This difference may be attributed to several reasons. The first might be the difference in forest definition. The forest cover map of this study, JAXA FNF, and the JAXA FNF v2 forests all follow the FAO forest definition, whereas NLCD 2016 uses a more restrictive forest definition (canopy coverage > 20%, canopy height > 5 m). Consequently, NLCD 2016 reported a smaller forested area (39,783 km^2) than this study (52,431 km^2). For the OKESM map, the forest is defined as having a canopy coverage of over 25% and a tree height of over 4 m. The forested area of 50,302 km^2, which was close to this study (51,852 km^2). The second reason might be the difference in data sources. Both JAXA FNF and JAXA FNF v2 were generated using strong backscatter signals in HV from forests. NLCD 2016 and OKESM both utilized several cloud-free Landsat images chosen from separate years or a multi-year collection. However, the forests delineated in these datasets were prone to confusion with other types, such as shrublands or recently opened woodlands. This may lead to inaccurate estimates of forested areas, unsuitable for mapping rapidly changing forests, such as those in southeastern Oklahoma (Tran et al., 2016). The third reason might be the difference in forest mapping algorithms. All six forest datasets were generated utilizing the decision tree approach, employing diverse and intricate processing techniques and thresholds. For instance, the HV threshold (> −14.2 dB) of the JAXA FNF map (Shimada et al., 2014) exceeded the threshold (HV > −19 dB) used in this study. Consequently, the PALSAR/Landsat forest map in 2015 tended to exhibit more 6,886 km^2 (~13.3%) forest distribution than the JAXA FNF map in 2015.

4.3 Implication and future work

This study generated annual maps of evergreen forests in Oklahoma, and we found a slight increase in evergreen forest areas from 2017 to 2020. Evergreen forests in Oklahoma are largely dominated by juniper (*Juniperus* spp.) that have been steadily encroaching into grassland areas across the state due to several man-made factors (Wang et al., 2018) and pine trees (*Pinus* spp.) that are primarily restricted to the southeastern Oklahoma as both natural and plantation forests. Evergreen plants, and specifically Junipers, are experiencing a growth rate in Oklahoma that is five to seven times higher than in other parts of the United States of America (Zou et al., 2016). The annual forest maps from this study could be used to analyze WPE dynamics in these years. Since this methodology cannot distinguish between pine plantations and juniper WPE, it is necessary to identify the spatial-temporal dynamics and stand ages of WPE through annual forest maps that combine with Landsat images from the 1980s to the present.

5 Conclusions

In Oklahoma, considerable uncertainties persist in estimating forest areas, characterizing spatial patterns and their changes. We generated and evaluated annual maps of forest cover, evergreen, deciduous, and mixed forests from 2015 to 2021 using an innovative methodology combining PALSAR-2, Landsat, and LiDAR datasets. Forests and non-forests cover 29% and 71% of the Oklahoma area, respectively, and forest area slightly increased (~1.9%, 987 km^2) from 2016 to 2020. Evergreen forests were mainly distributed in southeastern Oklahoma with no significant change, and mixed forests are concentrated in central and northeast regions with a slight increase (~1.7%, 464 km^2). The PALSAR/Landsat forest cover maps had relatively high accuracy as evaluated by both ICESat-2 and GEDI samples. The average percentage of ICESat-2 and GEDI samples within forested areas that met the FAO forest definition

was 95.7% and 76.2%, respectively. Furthermore, the PALSAR/Landsat forest cover maps and other satellite-based products had relatively high spatial distribution consistency for central, southeastern, and northeastern Oklahoma, but significant disagreement and uncertainty in western Oklahoma. The total forest area in this study in 2017 (51,916 km^2) was moderately higher (7.2%) than FIA statistics data (48,202 km^2). The annual PALSAR/Landsat forest maps produced in this study could be used as a new dataset to support policy implementation for local forest conservation and management. More studies are needed to classify tree species, such as evergreen juniper trees to investigate the processes and drivers of woody plant encroachment in this region over the past decades.

Acknowledgments This study was supported in part by research grants from the US National Science Foundation (OIA-1946093, OIA-1920946).

Competing interests The authors declare that they have nocompetinginterests.

Electronic Supplementary Material is available in the online version of this article at http://dx.doi.org/10.1007/s11707-025-1151-4 and is accessible for authorized users.

References

Adhikari A, Masters R E, Mainali K P, Zou C B, Joshi O, Will R E (2021). Management and climate variability effects on understory productivity of forest and savanna ecosystems in Oklahoma, USA. Ecosphere, 12(6): e03576

Ahmad A, Gilani H, Ahmad S R (2021). Forest aboveground biomass estimation and mapping through high-resolution optical satellite imagery—A literature review. Forests, 12(7): 914

Chen B, Xiao X, Ye H, Ma J, Doughty R, Li X, Zhao B, Wu Z, Sun R, Dong J, Qin Y, Xie G (2018). Mapping forest and their spatial–temporal changes from 2007 to 2015 in tropical hainan island by integrating ALOS/ALOS-2 L-Band SAR and landsat optical images. IEEE J Sel Top Appl Earth Obs Remote Sens, 11(3): 852–867

Diamond D D, Elliott L F (2015). Oklahoma ecological systems mapping interpretive booklet: methods, short type descriptions, and summary results. Oklahoma Department of Wildlife Conservation, Norman

Dooley K (2017). Forests of Oklahoma, 2015. Resource Update FS–126. Asheville, NC: U.S. Department of Agriculture Forest Service, Southern Research Station

Dubayah R, Hofton M, Blair J, Armston J, Tang H, Luthcke S (2021a). GEDI L2A Elevation and Height Metrics Data Global Footprint Level V002.

Dubayah R, Tang H, Armston J, Luthcke S, Hofton M, Blair J (2021b). GEDI L2B Canopy Cover and Vertical Profile Metrics Data Global Footprint Level V002.

Duncanson L, Neuenschwander A, Hancock S, Thomas N, Fatoyinbo T, Simard M, Silva C A, Armston J, Luthcke S B, Hofton M, Kellner J R, Dubayah R (2020). Biomass estimation from simulated GEDI, ICESat-2 and NISAR across environmental gradients in Sonoma County, California. Remote Sens Environ, 242: 111779

El Moussawi I, Ho Tong Minh D, Baghdadi N, Abdallah C, Jomaah J, Strauss O, Lavalle M, Ngo Y N (2019). Monitoring tropical forest structure using sar tomography at L- and P-band. Remote Sens (Basel), 11(16): 1934

Felipe-Lucia M R, Soliveres S, Penone C, Fischer M, Ammer C, Boch S, Boeddinghaus R S, Bonkowski M, Buscot F, Fiore-Donno A M, Frank K, Goldmann K, Gossner M M, Hölzel N, Jochum M, Kandeler E, Klaus V H, Kleinebecker T, Leimer S, Manning P, Oelmann Y, Saiz H, Schall P, Schloter M, Schöning I, Schrumpf M, Solly E F, Stempfhuber B, Weisser W W, Wilcke W, Wubet T, Allan E (2020). Land-use intensity alters networks between biodiversity, ecosystem functions, and services. Proc Natl Acad Sci USA, 117(45): 28140–28149

García P R, Scaccia L, Salvati L (2023). An accuracy assessment of three forest cover databases in Colombia. Environ Ecol Stat, 30(3): 443–475

Gong P, Wang J, Yu L, Zhao Y, Zhao Y, Liang L, Niu Z, Huang X, Fu H, Liu S, Li C, Li X, Fu W, Liu C, Xu Y, Wang X, Cheng Q, Hu L, Yao W, Zhang H, Zhu P, Zhao Z, Zhang H, Zheng Y, Ji L, Zhang Y, Chen H, Yan A, Guo J, Yu L, Wang L, Liu X, Shi T, Zhu M, Chen Y, Yang G, Tang P, Xu B, Giri C, Clinton N, Zhu Z, Chen J, Chen J (2013). Finer resolution observation and monitoring of global land cover: first mapping results with Landsat TM and ETM+ data. Int J Remote Sens, 34(7): 2607–2654

Homer C, Dewitz J, Jin S, Xian G, Costello C, Danielson P, Gass L, Funk M, Wickham J, Stehman S, Auch R, Riitters K (2020). Conterminous United States land cover change patterns 2001–2016 from the 2016 national land cover database. ISPRS J Photogramm Remote Sens, 162: 184–199

Hoover C M, Bush R, Palmer M, Treasure E (2020). Using forest inventory and analysis data to support national forest management: regional case studies. J For, 118(3): 313–323

Kaur R, Joshi O, Will R E (2020). The ecological and economic determinants of eastern redcedar (*Juniperus virginiana*) encroachment in grassland and forested ecosystems: a case study from Oklahoma. J Environ Manage, 254: 109815

Kulkarni S C, Rege P P (2020). Pixel level fusion techniques for SAR and optical images: a review. Inf Fusion, 59: 13–29

Liu A, Cheng X, Chen Z (2021). Performance evaluation of GEDI and ICESat-2 laser altimeter data for terrain and canopy height retrievals. Remote Sens Environ, 264: 112571

Lu J, Huang C, Tao X, Gong W, Schleeweis K (2022). Annual forest disturbance intensity mapped using Landsat time series and field inventory data for the conterminous United States (1986–2015). Remote Sens Environ, 275: 113003

Luo L, Wang X, Guo H, Lasaponara R, Zong X, Masini N, Wang G, Shi P, Khatteli H, Chen F, Tariq S, Shao J, Bachagha N, Yang R, Yao Y (2019). Airborne and spaceborne remote sensing for archaeological and cultural heritage applications: a review of the

century (1907–2017). Remote Sens Environ, 232: 111280

Ma C, Qian Y, Li K, Dou X, Shen H, Tang H, Qiu S, Zhang L, Jia Y, Ou-Yang G (2023). Temperature and emissivity retrieval from hyperspectral thermal infrared data using dictionary-based sparse representation for emissivity. IEEE Trans Geosci Remote Sens, 61: 5002016

Markus T, Neumann T, Martino A, Abdalati W, Brunt K, Csatho B, Farrell S, Fricker H, Gardner A, Harding D, Jasinski M, Kwok R, Magruder L, Lubin D, Luthcke S, Morison J, Nelson R, Neuenschwander A, Palm S, Popescu S, Shum C K, Schutz B E, Smith B, Yang Y, Zwally J (2017). The Ice, Cloud, and land Elevation Satellite-2 (ICESat-2): science requirements, concept, and implementation. Remote Sens Environ, 190: 260–273

Neuenschwander A, Pitts K (2019). The ATL08 land and vegetation product for the ICESat-2 Mission. Remote Sens Environ, 221: 247–259

Patterson P L, Healey S P, Ståhl G, Saarela S, Holm S, Andersen H E, Dubayah R O, Duncanson L, Hancock S, Armston J, Kellner J R, Cohen W B, Yang Z (2019). Statistical properties of hybrid estimators proposed for GEDI—NASA's global ecosystem dynamics investigation. Environ Res Lett, 14(6): 065007

Potapov P, Li X, Hernandez-Serna A, Tyukavina A, Hansen M C, Kommareddy A, Pickens A, Turubanova S, Tang H, Silva C E, Armston J, Dubayah R, Blair J B, Hofton M (2021). Mapping global forest canopy height through integration of GEDI and Landsat data. Remote Sens Environ, 253: 112165

Qin Y, Xiao X, Dong J, Zhang G, Roy P S, Joshi P K, Gilani H, Murthy M S R, Jin C, Wang J, Zhang Y, Chen B, Menarguez M A, Biradar C M, Bajgain R, Li X, Dai S, Hou Y, Xin F, Moore B III (2016a). Mapping forests in monsoon Asia with ALOS PALSAR 50-m mosaic images and MODIS imagery in 2010. Sci Rep, 6(1): 20880

Qin Y, Xiao X, Dong J, Zhang G, Shimada M, Liu J, Li C, Kou W, Moore B III (2015). Forest cover maps of China in 2010 from multiple approaches and data sources: PALSAR, Landsat, MODIS, FRA, and NFI. ISPRS J Photogramm Remote Sens, 109: 1–16

Qin Y, Xiao X, Dong J, Zhang Y, Wu X, Shimabukuro Y, Arai E, Biradar C, Wang J, Zou Z, Liu F, Shi Z, Doughty R, Moore B III (2019). Improved estimates of forest cover and loss in the Brazilian Amazon in 2000–2017. Nat Sustain, 2(8): 764–772

Qin Y, Xiao X, Dong J, Zhou Y, Wang J, Doughty R B, Chen Y, Zou Z, Moore B III (2017). Annual dynamics of forest areas in South America during 2007–2010 at 50-m spatial resolution. Remote Sens Environ, 201: 73–87

Qin Y, Xiao X, Wang J, Dong J, Ewing K, Hoagland B, Hough D J, Fagin T D, Zou Z, Geissler G L, Xian G Z, Loveland T R (2016b). Mapping annual forest cover in sub-humid and semi-arid regions through analysis of Landsat and PALSAR Imagery. Remote Sens (Basel), 8(11): 933

Qin Y, Xiao X, Wigneron J P, Ciais P, Canadell J G, Brandt M, Li X, Fan L, Wu X, Tang H, Dubayah R, Doughty R, Crowell S, Zheng B, Moore B III (2022). Large loss and rapid recovery of vegetation cover and aboveground biomass over forest areas in Australia during 2019–2020. Remote Sens Environ, 278: 113087

Quegan S, Le Toan T, Yu J J, Ribbes F, Floury N (2000). Multitemporal ERS SAR analysis applied to forest mapping. IEEE Trans Geosci Remote Sens, 38(2): 741–753

Reiche J, Hamunyela E, Verbesselt J, Hoekman D, Herold M (2018). Improving near-real time deforestation monitoring in tropical dry forests by combining dense Sentinel-1 time series with Landsat and ALOS-2 PALSAR-2. Remote Sens Environ, 204: 147–161

Sexton J O, Song X P, Feng M, Noojipady P, Anand A, Huang C, Kim D H, Collins K M, Channan S, DiMiceli C, Townshend J R (2013). Global, 30-m resolution continuous fields of tree cover: Landsat-based rescaling of MODIS vegetation continuous fields with lidar-based estimates of error. Int J Digit Earth, 6(5): 427–448

Shakya A, Biswas M, Pal M (2022). Fusion and classification of multi-temporal SAR and optical imagery using convolutional neural network. Int J Image Data Fusion, 13(2): 113–135

Sheldon S, Xiao X, Biradar C (2012). Mapping evergreen forests in the Brazilian Amazon using MODIS and PALSAR 500-m mosaic imagery. ISPRS J Photogramm Remote Sens, 74: 34–40

Shimada M, Itoh T, Motooka T, Watanabe M, Shiraishi T, Thapa R, Lucas R (2014). New global forest/non-forest maps from ALOS PALSAR data (2007–2010). Remote Sens Environ, 155: 13–31

Stehman S V, Foody G M (2019). Key issues in rigorous accuracy assessment of land cover products. Remote Sens Environ, 231: 111199

Tinkham W T, Mahoney P R, Hudak A T, Domke G M, Falkowski M J, Woodall C W, Smith A M S (2018). Applications of the United States forest inventory and analysis dataset: a review and future directions. Can J For Res, 48(11): 1251–1268

Tran T V, de Beurs K M, Julian J P (2016). Monitoring forest disturbances in Southeast Oklahoma using Landsat and MODIS images. Int J Appl Earth Obs Geoinf, 44: 42–52

Wang J, Xiao X, Qin Y, Dong J, Geissler G, Zhang G, Cejda N, Alikhani B, Doughty R B (2017). Mapping the dynamics of eastern redcedar encroachment into grasslands during 1984–2010 through PALSAR and time series Landsat images. Remote Sens Environ, 190: 233–246

Wang J, Xiao X, Qin Y, Dong J, Zhang G, Yang X, Wu X, Biradar C, Hu Y (2024). Annual forest maps in the contiguous United States during 2015-2017 from analyses of PALSAR-2 and Landsat images. Earth System Science Data, 16(10): 4619–4639

Wang J, Xiao X, Qin Y, Doughty R B, Dong J, Zou Z (2018). Characterizing the encroachment of juniper forests into sub-humid and semi-arid prairies from 1984 to 2010 using PALSAR and Landsat data. Remote Sens Environ, 205: 166–179

Xiao X, Biradar C M, Czarnecki C, Alabi T, Keller M (2009). A simple algorithm for large-scale mapping of evergreen forests in tropical America, Africa and Asia. Remote Sens (Basel), 1(3): 355–374

Xiao X, Dorovskoy P, Biradar C, Bridge E (2011). A library of georeferenced photos from the field. Eos (Wash DC), 92(49): 453–454

Xu Y, Lu Z, Bürgmann R, Hensley S, Fielding E, Kim J (2023). P-

band SAR for ground deformation surveying: advantages and challenges. Remote Sens Environ, 287: 113474

Yang J, Will R, Zhai L, Zou C (2024). Future climate change shifts the ranges of major encroaching woody plant species in the southern great plains, USA. Earth's Future, 12: e2024EF004520

Yu Q, Ryan M G, Ji W, Prihodko L, Anchang J Y, Kahiu N, Nazir A, Dai J, Hanan N P (2024). Assessing canopy height measurements from ICESat-2 and GEDI orbiting LiDAR across six different biomes with G-LiHT LiDAR. Environ Res: Ecology, 3(2): 025001

Zhang D, Wang H, Wang X, Lü Z (2020). Accuracy assessment of the global forest watch tree cover 2000 in China. Int J Appl Earth Obs Geoinf, 87: 102033

Zhu X, Nie S, Wang C, Xi X, Lao J, Li D (2022). Consistency analysis of forest height retrievals between GEDI and ICESat-2. Remote Sens Environ, 281: 113244

Zou C B, Qiao L, Wilcox B P (2016). Woodland expansion in central Oklahoma will significantly reduce streamflows – a modelling analysis. Ecohydrology, 9(5): 807–816